Applied Mathematical Modelling 36 (2012) 2237–2252

Contents lists available at SciVerse ScienceDirect

Applied Mathematical Modelling

journal homepage: www.elsevier.com/locate/apm

Numerical evaluation of two recoloring operators for an immiscible two-phase flow lattice Boltzmann model

Sébastien Leclaire *, Marcelo Reggio, Jean-Yves Trépanier

Department of Mechanical Engineering, École Polytechnique, 2500, Chemin de Polytechnique, Montreal, Quebec, Canada H3T 1J4

ARTICLE INFO

Article history:
Received 5 May 2011
Received in revised form 3 August 2011
Accepted 10 August 2011
Available online 23 August 2011

Keywords:
Lattice Boltzmann method
Immiscible two-phase flow
Recoloring operators
Lattice pinning
Surface tension
Layered Poiseuille flow

ABSTRACT

The lattice Boltzmann method is applied to the study of immiscible two-phase flows using a Rothman–Keller-type (RK) model. The focus is on the algorithm proposed by Latva-Kokko and Rothman, which has been modified and integrated into the Reis and Phillips model, which belongs to the RK family. A key element of the RK model is the recoloring step applied at the interface of two fluids, at which the fluids are separated and sent to their own region. When convection is weak, the interface in the Reis and Phillips model suffers from "lattice pinning", which is a problem that may prevent the interface from moving. While the recoloring algorithm proposed by Latva-Kokko and Rothman diminishes this problem, it was not used in the work of Reis and Phillips. This is the framework in which the present study has been conducted. Its scope is twofold: first, to integrate and adapt the Latva-Kokko and Rothman recoloring algorithms for reducing the lattice pinning problem found in the Reis and Phillips model; and second, to conduct a set of numerical tests to show that the combination of the two algorithms leads to an improvement in the quality of the results, along with a better convergence. The context of the work is two-dimensional, with the D2Q9 lattice used as the basic computational element.

1. Introduction

The recently devised lattice Boltzmann method (LBM), historically derived from cellular automata [1,2], has been shown to be well suited to simulating complex flows, including immiscible multiphase flows [3–9]. These include the formation and coalescence of drops [10,11], rising bubbles [12–14], flows of immiscible fluids in porous media [15–18], blood flow [19], and the dissolution of liquid droplets in another liquid [20], among others. Comparisons with experiments have also been performed [12,16,10].

Models for lattice Boltzmann immiscible multiphase flows can generally be classified in five categories: the Rothman–Keller (RK) [19,21,4,5,3,6–8,22,16,10,23], Shan–Chen (SC) [20,24,25,9], free energy (FE) [12,26,15,14], mean-field (MF) [27,28], and field mediator (FM) methods [29]. In this study, the Reis and Phillips model [8], which belongs to the RK family and is based on color gradients to maintain sharp interfaces, has been adopted. The advantage of this approach is the flexibility with which the model's parameters can be chosen. It allows independent control of the surface tension, density ratio, and viscosity ratio of the various fluids on either side of an interface, as well as control of the contact angle and the wetting behavior of the solid phases [5]. With the representation of Reis and Phillips [8], higher density ratios can be tackled than with other RK models.

Some years ago, Hou et al. [30] compared the RK and SC models. One of the conclusions of their study was that the SC model provides better results, as it produces less intense spurious currents at the interface. In our current work, we will

* Corresponding author.
E-mail address: sebastien.leclaire@polymtl.ca (S. Leclaire).

0307-904X/$ - see front matter © 2011 Elsevier Inc. All rights reserved.
doi:10.1016/j.apm.2011.08.027

show that, when Latva-Kokko's recoloring operator is adapted to the Reis and Phillips RK model, a significant reduction in the spurious currents is achieved. Ginzbourg and Adler [21] also showed that, with an RK model, these currents can be removed completely with a particular choice of eigenvalues in the collision operator. However, these authors only demonstrate that the improvement is valid for a simple test case. The above-referenced RK-based models follow Gunstensen and Rothman's [45] Ph.D. thesis, which mentions that the lattice Boltzmann representation recovers Galilean invariance with a proper assignment of the rest equilibrium particles. The ability to simulate flow with a variable density ratio was introduced by Grunau et al. [3], who presented unsteady flow simulations with density ratios up to 10. Since then, the ability of the RK family to simulate flows with a variable density ratio has been investigated very little. In one study [16], Tölke reported a density ratio of 30 for a steady flow simulation, and a density ratio of 4 for an unsteady flow simulation. With the Reis and Phillips representation [8], higher density ratios can be tackled than with other RK models, i.e. a density ratio of up to 18.5 has been reported for an unsteady simulation. In addition, their approach has been shown to be compatible with the macroscopic equations for two-phase flows.

The models in the SC family also have the advantage of being easy to implement and capable of readily simulating fluids with a high-density ratio, but the various parameters of the model cannot be chosen independently [22]. The SC family allows the use of non-ideal equations of state by abandoning the conservation of local momentum and respecting only the conservation of momentum in a global sense [31]. Methods such as the FE type face other kinds of problems; for example, they do not respect Galilean invariance [22]. Nevertheless, the FE methods have two advantages: they can produce interfaces as thin as two lattice units [18], and they allow the use of a van der Waals equation of state for gas flows, instead of the ideal gas law [32]. The three families, RK, SC, and FE, are theoretically able to simulate an arbitrary number of fluid components [19,9,33]. The MF methods simulate interparticle attraction in the same way as the Coulomb interaction is treated in the Vlasov equation [27]. These models can simulate thermodynamically consistent liquid–vapor systems, where the SC models fail [34]. Based on the MF methods and stable discretization of the lattice Boltzmann equation, a recent model from Lee et al. [35] was introduced and shows promising results. They were able to simulate non-ideal gaseous systems with increased numerical stability for a large density ratio O(1000). The FM methods use null-mass particles, the only role of which is to invert the momentum of lattice particles in the transition layer to segregate fluids of different colors [29]. They have the advantage of being able to incorporate binary diffusivity, and this method can also, therefore, be adapted to simulate miscible fluids.

In our study here, numerical experiments were conducted, closely following the work of Reis and Phillips, to validate the integration of the recoloring algorithm of Ref. [7] into the model of Ref. [8]. These include the surface tension predicted for a planar interface, the Laplace equation for surface tension, and the Poiseuille equation for a layered immiscible fluid with different viscosities. All three test cases are compared with theoretical results. As a fourth test case, the coalescence of two circular bubbles of the same density immersed in a fluid of a higher/lower density is discussed. Finally, a numerical experiment to test the problem of lattice pinning is proposed and investigated. We should mention that another recoloring algorithm has been presented in Ref. [16], but is not studied in this work.

2. Lattice Boltzmann immiscible two-phase model

For the Reis and Phillips model [8] in two dimensions, there are two sets of distribution functions, one for each fluid, moving on a D2Q9 grid with the velocity vectors $\overrightarrow{c_i}$. With $\theta_i = \frac{\pi}{4}(4-i)$, the velocity vectors are defined as:

$$\overrightarrow{c_i} = \begin{cases} (0,0), & i = 1, \\ [\sin(\theta_i), \cos(\theta_i)], & i = 2,4,6,8, \\ [\sin(\theta_i), \cos(\theta_i)]\sqrt{2}, & i = 3,5,7,9. \end{cases} \tag{1}$$

The distribution functions for a fluid of color k (with $k = r$ for red and $k = b$ for blue) are noted $N_i^k(\vec{x},t)$, while $N_i(\vec{x},t)$ is used for the sum $N_i^r(\vec{x},t) + N_i^b(\vec{x},t)$. If the time step is $\Delta t = 1$, the algorithm from [8] uses the following evolution equation:

$$N_i^k(\vec{x} + \overrightarrow{c_i}, t+1) = N_i^k(\vec{x},t) + \Omega_i^k(N_i^k(\vec{x},t)), \tag{2}$$

where the collision operator Ω_i^k is the result of the combination of three sub-operators (similar to Ref. [16]):

$$\Omega_i^k = (\Omega_i^k)^{(3)}\left[(\Omega_i^k)^{(1)} + (\Omega_i^k)^{(2)}\right]. \tag{3}$$

In the algorithm, the evolution equation is solved in four steps with operator splitting, as follows:

1. Single-phase collision operator:

$$N_i^k(\vec{x}, t_*) = (\Omega_i^k)^{(1)}(N_i^k(\vec{x},t)).$$

2. Two-phase collision operator (perturbation):

$$N_i^k(\vec{x}, t_{**}) = (\Omega_i^k)^{(2)}(N_i^k(\vec{x}, t_*)).$$

3. Two-phase collision operator (recoloring):

$$N_i^k(\vec{x}, t_{***}) = (\Omega_i^k)^{(3)}(N_i^k(\vec{x}, t_{**})).$$

4. Streaming operator:

$$N_i^k(\vec{x}+\vec{c_i},t+1)=N_i^k(\vec{x},t_{***}).$$

2.1. Single-phase collision operator

The first sub-operator $(\Omega_i^k)^{(1)}$ is the standard BGK operator of the single-phase LBM, where the distribution functions are relaxed towards a local equilibrium in which ω_k denotes the relaxation factor:

$$(\Omega_i^k)^{(1)}(N_i^k)=N_i^k-\omega_k\left(N_i^k-N_i^{k(e)}\right). \tag{4}$$

A few details concerning this operator are the following: The density of the fluid k is given by the first moment of the distribution functions:

$$\rho_k=\sum_i N_i^k=\sum_i N_i^{k(e)}, \tag{5}$$

where the superscript (e) denotes equilibrium. The total fluid density is given by $\rho=\rho_r+\rho_b$, while the total momentum is defined as the second moment of the distribution functions:

$$\rho\vec{u}=\sum_i\sum_k N_i^k\vec{c_i}=\sum_i\sum_k N_i^{k(e)}\vec{c_i} \tag{6}$$

in which $\vec{u}$ is the total and local velocity of the fluid. The equilibrium functions are defined by [8]:

$$N_i^{k(e)}=\rho_k\left(\phi_i^k+W_i\left[3\vec{c_i}\cdot\vec{u}+\frac{9}{2}(\vec{c_i}\cdot\vec{u})^2-\frac{3}{2}(\vec{u})^2\right]\right). \tag{7}$$

These equilibrium distribution functions, $N_i^{k(e)}$, are chosen to respect the conservation of mass and momentum [8]. The weights W_i are those of a standard D2Q9 lattice:

$$W_i=\begin{cases}4/9, & i=1,\\ 1/9, & i=2,4,6,8,\\ 1/36, & i=3,5,7,9.\end{cases} \tag{8}$$

Moreover,

$$\phi_i^k=\begin{cases}\alpha_k, & i=1,\\ (1-\alpha_k)/5, & i=2,4,6,8,\\ (1-\alpha_k)/20, & i=3,5,7,9.\end{cases} \tag{9}$$

As introduced in [3], to obtain a stable interface, the density ratio γ needs to be taken as follows:

$$\gamma=\frac{\rho_r}{\rho_b}=\frac{1-\alpha_b}{1-\alpha_r}. \tag{10}$$

Without loss of generality, in this paper $\rho_r\geqslant\rho_b$. The pressure of the fluid of color k is:

$$p^k=\frac{3\rho_k(1-\alpha_k)}{5}=\rho_k(c_s^k)^2 \tag{11}$$

where, in the above expressions, either α_r or α_b represents a free parameter, and c_s^k is the sound speed in the fluid of color k [20,8]. These parameters are important when the density ratio γ is large [8]. Theoretically, the constraint $\alpha_b\leqslant 1$ must be respected in order to avoid negative pressures. It is also possible to show that $0\leqslant\alpha_b\leqslant\alpha_r\leqslant 1$ is always true when $\rho_r\geqslant\rho_b$ and $0\leqslant\alpha_b\leqslant 1$.

The relaxation parameters ω_k are chosen so that the evolution Eq. (2) respects the macroscopic equations for single-phase flow in the single-phase regions [8]. This parameter is a function of the fluid kinematic viscosity ν_k, given by $\omega_k=1/(3\nu_k+\frac{1}{2})$. As introduced in [3], when the viscosities of the fluids are different, an interpolation is applied to define the parameter ω_k at the interface. To do this, it is necessary to introduce the color field:

$$\psi=\frac{\rho_r-\rho_b}{\rho_r+\rho_b}. \tag{12}$$

The color field ψ is a function with its image between -1 and 1. It takes the value 1 or -1, depending on whether it is evaluated at a position that contains only red fluid or only blue fluid. In an interface, the color field is obviously between -1 and 1. The relaxation factor ω_k in Eq. (4) is replaced by ω:

$$\omega = \begin{cases} \omega_r, & \psi > \delta, \\ f_r(\psi), & \delta \geqslant \psi > 0, \\ f_b(\psi), & 0 \geqslant \psi \geqslant -\delta, \\ \omega_b, & \psi < -\delta \end{cases} \tag{13}$$

in which δ is a free parameter and

$$\begin{aligned} f_r(\psi) &= \chi + \eta\psi + \kappa\psi^2, \\ f_b(\psi) &= \chi + \lambda\psi + \upsilon\psi^2 \end{aligned} \tag{14}$$

with

$$\begin{aligned} \chi &= 2\omega_r\omega_b/(\omega_r + \omega_b), \\ \eta &= 2(\omega_r - \chi)/\delta, \\ \kappa &= -\eta/(2\delta), \\ \lambda &= 2(\chi - \omega_b)/\delta, \\ \upsilon &= \lambda/(2\delta). \end{aligned} \tag{15}$$

The free parameter δ is required to calculate ω, and is chosen to be 0.1 for all the simulations in this paper. It is a parameter that influences the thickness of the interface when the fluid viscosities are different [8]. The larger δ, the thicker the fluid interface. If the fluid viscosities are the same, the parameter δ does not have an impact on the solution, because, in this case, $\omega = \omega_r = \omega_b$.

2.2. Perturbation operator

In the RK model, surface tension is modeled by means of the perturbation operator [5,6,8]. First, the color gradient in terms of the color difference is defined by:

$$\overrightarrow{F}(\vec{x}) = \sum_i \overrightarrow{c_i}\left(\rho_r(\vec{x} + \overrightarrow{c_i}) - \rho_b(\vec{x} + \overrightarrow{c_i})\right). \tag{16}$$

The color gradient direction is an approximation of the perpendicular to the interface between the fluids. This perturbation operator is defined by:

$$(\Omega_i^k)^{(2)}(N_i^k) = N_i^k + \frac{A_k}{2}|\overrightarrow{F}|\left[W_i\frac{(\overrightarrow{F}\cdot\overrightarrow{c_i})^2}{|\overrightarrow{F}|^2} - B_i\right] \tag{17}$$

where

$$B_i = \begin{cases} -4/27, & i = 1, \\ 2/27, & i = 2,4,6,8, \\ 5/108, & i = 3,5,7,9. \end{cases} \tag{18}$$

Reis and Phillips [8] have shown that this operator complies with the macroscopic equations for two-phase flows. It handles the coupling between the two fluids, with the free parameters A_k chosen to model the surface tension. Although this operator generates the surface tension, it does not guarantee the fluid's immiscibility. To minimize the mixing of the two fluids, the recoloring operator $(\Omega_i^k)^{(3)}$ must be introduced.

2.3. Recoloring operator

2.3.1. Original Reis recoloring algorithm

This last operator is used to maximize the amount of red fluid at the interface sent to the red fluid region, and the amount of blue fluid sent to the blue fluid region, while respecting the conservation of mass and total momentum. Reis' model uses a recoloring method that produces a very thin interface, but, as recognized by the authors, it has the problem of lattice pinning [8]. By defining the color flux:

$$\overrightarrow{K}(\vec{x}) = \sum_i (N_i^r - N_i^b)\overrightarrow{c_i}, \tag{19}$$

the recoloring operator is used to maximize the work W performed by the color gradient against the color flux [5,8,2]:

$$W = \overrightarrow{K}\cdot\overrightarrow{F} \tag{20}$$

subject to the following equivalent constraints of mass and total momentum conservation:

$$\begin{aligned} N_i^r + N_i^b &= N_i \\ \sum_i N_i^r &= \rho_r \end{aligned} \tag{21}$$

The standard optimization techniques, such as Lagrange multipliers, cannot be used to solve this problem [8]. Instead, the usual RK model method is used, which consists of maximizing the number of red particles sent in the direction of the color gradient $\vec{F}$, while respecting the constraints given in Eq. (21). This is achieved as follows.

First, the $\vec{c_i}$ directions are reordered, with the first one pointing in the direction closest to $\vec{F}$, then the second closest is placed, and so on. The vector $\vec{c_1}$ is located at the center of the nine directions. Then, a maximum mass of red fluid is sent in the direction closest to $\vec{F}$, always within the constraints imposed by Eq. (21). Using the amount of red fluid remaining, the maximum quantity of red fluid is sent in the second direction closest to $\vec{F}$, still respecting the constraints required by Eq. (21). This process is repeated until all the red fluid has been redistributed. In this paper, this operator is called *recoloring operator I*.

2.3.2. Original Latva-Kokko and modified recoloring algorithm

In the model proposed by Latva-Kokko and Rothman [7], the recoloring operator is defined as follows:

$$(\Omega_i^r)^{(3)}(N_i^r) = \frac{\rho_r}{\rho} N_i + \beta \frac{\rho_r \rho_b}{\rho^2} \cos(\varphi_i) N_i^{(e)}(\rho, 0), \tag{22}$$

$$(\Omega_i^b)^{(3)}(N_i^b) = \frac{\rho_b}{\rho} N_i - \beta \frac{\rho_r \rho_b}{\rho^2} \cos(\varphi_i) N_i^{(e)}(\rho, 0), \tag{23}$$

where the color-blind equilibrium function is $N_i^{(e)}$, and therefore the recoloring operator is defined for a constant value of α_r and α_b. Thus, when combining the Latva-Kokko and Rothman [7] recoloring operator with the Reis and Phillips model [8], it is important to take into account that the sound speed is a free parameter in the Reis and Phillips model. In this respect, a contribution of this paper is the adaptation of the Latva-Kokko recoloring operator for a variable speed of sound. The new recoloring operator takes the following form:

$$(\Omega_i^r)^{(3)}(N_i^r) = \frac{\rho_r}{\rho} N_i + \beta \frac{\rho_r \rho_b}{\rho^2} \cos(\varphi_i) \sum_k N_i^{k(e)}(\rho_k, 0, \alpha_k), \tag{24}$$

$$(\Omega_i^b)^{(3)}(N_i^b) = \frac{\rho_b}{\rho} N_i - \beta \frac{\rho_r \rho_b}{\rho^2} \cos(\varphi_i) \sum_k N_i^{k(e)}(\rho_k, 0, \alpha_k), \tag{25}$$

where β is a free parameter and $\cos(\varphi_i)$ is the cosine of the angle between the color gradient $\vec{F}$ and the direction $\vec{c_i}$. The color-blind equilibrium distributions $N_i^{(e)}$ in Eqs. (22) and (23) are replaced with the sum of the equilibrium distributions of each fluid $N_i^{k(e)}$ in Eqs. (24) and (25), and are evaluated using the respective value of α_k and a zero velocity. The value of $\cos(\varphi_1)$ must equal 0 in order to conserve mass. Also, the parameter β must be between 0 and 1 to ensure that the distribution functions remain positive [7]. It is important to mention that other factors in a simulation could lead to negative distribution functions. Parameter β influences the thickness of the interface: the smaller its value, the thicker the interface. The value of β used in this paper is 0.99, unless otherwise stated. The recoloring operator defined by Eqs. (24) and (25) is called *recoloring operator II* in this paper.

3. Numerical results

The simulations were performed with a single-threaded MATLAB program running on a desktop equipped with an Intel core i7 970 CPU. In our setting, this processor can compute, on average, approximately 70 and 90 time steps per second for recoloring operators I and II respectively, for a lattice with 100×100 sites and periodic boundary conditions. It should be noted that the code was not intended to be particularly efficient. With it, we can nevertheless show that one advantage of the current recoloring operator (II) over the former operator (I) is the smaller computational cost per time step.

3.1. Planar interface

In a similar way to that shown in Ref. [8], we consider a planar interface parallel to the standard y-axis with a stationary fluid of a different color on each side of the interface. In such a case, and for the current model, it was shown by [8] that the surface tension is given by the following equation when measured from any line of integration perpendicular to the interface:

$$\sigma_{model} = \frac{(A_r + A_b)}{9\omega} \sum_{\vec{x}} |\vec{F}|. \tag{26}$$

Eq. (26) relates the surface tension in the model as a function of the color gradient and other parameters [8].

The mechanical definition of surface tension is [21,5,6,8]:

$$\sigma_{mec} = \int_{-\infty}^{+\infty} (P_N(z) - P_T(z))dz, \tag{27}$$

where P_N and P_T are the normal and tangential components of the pressure tensor. The z-axis is a line of integration perpendicular to the interface. By setting θ_z to be the angle of the z-axis with respect to the standard x-axis, and θ_i to be the relative angle between the x-axis and the vector $\overrightarrow{c_i}$, the components P_N and P_T are given by [8]:

$$\begin{aligned} P_N &= \sum_i N_i(|\overrightarrow{c_i}|\cos(\theta_i - \theta_z))^2, \\ P_T &= \sum_i N_i(|\overrightarrow{c_i}|\sin(\theta_i - \theta_z))^2. \end{aligned} \tag{28}$$

To perform numerical simulations on the planar interface, a computational domain of 64×64 sites is defined. Initially, all sites on the left-hand side of the computational domain are initialized with a red fluid using zero velocity equilibrium functions. The remaining sites are initialized in a same way, but with blue fluid. Periodic boundary conditions are used at each end of the computational domain. The viscosity of both fluids is $\nu_r = \nu_b = 1/6$. A value of $\alpha_b = 0.2$ is used. By directly applying Eqs. (26) and (27) on a horizontal line of integration, the surface tension measured is twice the desired value, as the line of integration passes through an interface twice. This is a consequence of the finite computational domain and the periodic boundary conditions.

The goal of this numerical experiment is to attest to the model's ability to create a surface tension between the fluids that is consistent with the mechanical definition. An additional goal is to show that it is possible to arrive at a desired surface tension by setting only the free parameters A_k of the model.

A total of 54 numerical simulations were conducted to study how the various parameters in the current model influence the surface tension. The total number of all possible combinations of input parameters is 54 ($2 \times 3 \times 3 \times 3$), as summarized in Table 1.

The stopping criterion applied to all planar interface simulations is:

$$\max_{\text{all distribution functions}} \left\{ |(N_i^k)^{(n)} - (N_i^k)^{(n-1)}| \right\} \leqslant \epsilon \tag{29}$$

with $\epsilon = 10^{-10}$ and n denoting the iteration number. If the criterion was not met within a maximum of 20,000 iterations, the simulations were stopped. The results after all 54 simulations showed that recoloring operator I failed to converge under the imposed convergence criterion. In contrast, operator II converges without difficulty. In fact, the maximum number of iterations required for all 54 simulations with operator II was 6000. Therefore, the limit of 20,000 iterations to allow convergence was appropriate for the planar interface problem. To demonstrate the better convergence of recoloring operator II over recoloring operator I, a plot showing the left-hand side of Eq. (29) versus the time step is presented in Fig. 1.

It was already known that the surface tension can be set in an RK model using only the free parameters. Work has been done by Reis and Phillips [8] and their predecessors to obtain the surface tension as a function of ρ, ω, A_r, and A_b. The expression obtained varies from one model to another, but they are always very similar. For the current model, by analyzing the simulation results of the previous setting, the value for the surface tension as a function of the various model parameters is generalized for the case of the variable density ratio (as in Ref. [16]):

$$\sigma_{predict} = \frac{4}{3}\frac{\frac{\rho_r+\rho_b}{2}}{\omega}(A_r + A_b) = \frac{4}{3}\frac{\left(1+\frac{1}{\gamma}\right)\frac{\rho_r}{2}}{\omega}(A_r + A_b). \tag{30}$$

Eq. (30) can therefore be used to approximately set the surface tension between the fluids.

Let us define the error corresponding to the ith simulation as follows:

$$\begin{aligned} E_i^m &= \frac{\left|\frac{\sigma_{mec}^i}{2} - \frac{\sigma_{model}^i}{2}\right|}{\frac{\sigma_{mec}^i}{2}}, \\ E_i^p &= \frac{\left|\frac{\sigma_{mec}^i}{2} - \sigma_{predict}^i\right|}{\frac{\sigma_{mec}^i}{2}} \end{aligned} \tag{31}$$

and compare the accuracy of recoloring operators I and II. Table 2 reports some relative errors for various simulation groups and norms. The first line compares the maximum surface tension errors obtained for all simulations when the density ratio γ

Table 1
Combination of parameters for the planar interface case.

Recoloring operator	$A_r = A_b$	ρ_r	γ
I	0.01	1	1
II	0.002	4	4
	0.0004	6	6

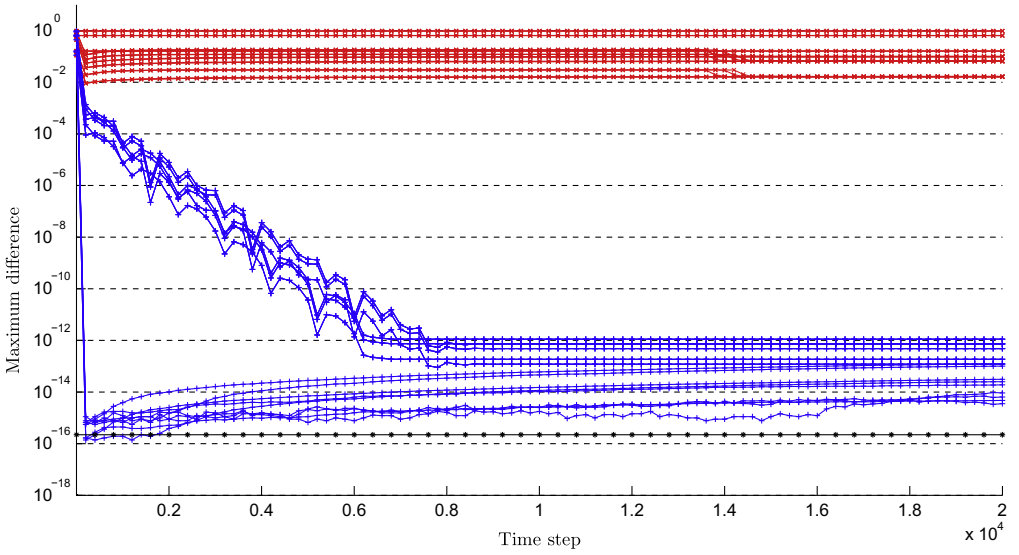

Fig. 1. Convergence of all planar interface simulations for recoloring operator I (red cross) and operator II (blue plus sign). Reference: machine epsilon (black star), *y*-axis is in log-scale. (For interpretation of the references to color in this figure legend, the reader is referred to the web version of this article.)

Table 2
Error comparison based on different norms for the planar interface problem.

	Recoloring I		Recoloring II	
	E^m (%)	E^p (%)	E^m (%)	E^p (%)
$\max\{E_i \mid \gamma = 1\}$	0	0	0	0
$\max\{E_i \mid \gamma \neq 1\}$	93.456	93.467	0	0.0095
$\min\{E_i \mid \gamma \neq 1\}$	7.5198	7.5524	0	0.0053
$\langle\{E_i \mid \gamma \neq 1\}\rangle$	51.222	51.261	0	0.0074

between the two fluids is unity. The next three lines are similar, except that the simulations with $\gamma \neq 1$ are considered to calculate the norms. Note that the integral in Eq. (27) is numerically evaluated with a simple midpoint method, with the lattice sites taken as the integration node. The symbol $\langle . \rangle$ stands for the average.

Regarding Table 2, it is important to note that, when $\gamma = 1$, the surface tension predicted by Eqs. (26) and (30) is the same as the mechanical surface tension, regardless of the recoloring operator. It has already been mentioned that it is the perturbation operator that introduces the surface tension in the numerical model. This means that, for the 18 simulations with $\gamma = 1$, neither recoloring operator introduces numerical errors into the surface tension generated by the perturbation operator. With $\gamma \neq 1$, recoloring operator I introduces a significant error in the surface tension produced by the perturbation operator. In contrast, with $\gamma \neq 1$, recoloring operator II performs better, in terms of both accuracy and the number of iterations required to reach convergence.

3.2. Steady bubble

The next numerical experiment involves a steady red bubble of radius R immersed in a blue fluid. The aim of this second numerical experiment is to verify whether or not the surface tension predicted by Eq. (30) is consistent with the Laplace equation [5,8]:

$$\sigma_{laplace} = R\Delta p, \tag{32}$$

where $\Delta p = p_{in} - p_{out}$ is the pressure jump between the inside and outside of the bubble. For these simulations, the computational domain is discretized with a lattice size of 128×128. Initially, the red fluid is placed at a distance of at most R from the center of the computational domain. The fluid is initialized with the zero velocity equilibrium distribution functions. The field is initialized in the same way for the blue fluid. Periodic boundary conditions are used at the four ends of the computational domain. A value of $\alpha_b = 0.6$ is used for all the steady bubble simulations. The pressures inside and outside the bubble are measured according to:

$$p_{in} = \frac{3}{5}\rho_{in}(1-\alpha_r)$$
$$p_{out} = \frac{3}{5}\rho_{out}(1-\alpha_b) \tag{33}$$

where

$$\rho_{in} = \langle\{\rho_r | \psi \geqslant \xi\}\rangle$$
$$\rho_{out} = \langle\{\rho_b | \psi \leqslant -\xi\}\rangle \tag{34}$$

For example, ρ_{in} is the average of the density ρ_r for all sites, such that the color field ψ is greater than or equal to ξ. The variable ξ is the nearest value to 1 in the following set: $\{1-0.1^n | n \leqslant 10\}$, such that there exists at least one site with $\psi \geqslant \xi$.

Let us denote by E_{I} the relative error between the surface tension $\sigma_{laplace}$ and $\sigma_{predict}$, with $\sigma_{predict}$ as a reference when a simulation was performed with recoloring operator I and by E_{II} if a simulation was performed with recoloring operator II. Table 3 illustrates the parameters and the errors resulting from the various simulations of the steady bubble.

Simulations not shown here revealed that, for $\gamma = 6$ and low surface tension, the Laplace equation leads to a negative surface tension when using recoloring operator I and $\alpha_b = 0.2$. It is important to note that recoloring operator II gives accurate results for $\alpha_b = 0.2$ and $\alpha_b = 0.6$.

Table 3 shows that the two recoloring operators produce results of similar accuracy when the density of the two fluids is equal. This result indicates the same behavior as in the simulation of the planar interface. In contrast, a large error is obtained by recoloring operator I when the density ratio is high and the surface tension is small. This indicates that recoloring operator II gives valid results for a wider range of parameters.

For the steady bubble experiment, we also looked at the effect of recoloring operators I and II on the spurious currents. These currents, found at the interface between two fluids, should be absent, and their origin is poorly understood. In the cellular automata literature [1], it has been mentioned that a recoloring operator of the form of recoloring operator II can reduce spurious currents. These results are confirmed for the current lattice Botlzmann model. Table 3 shows that recoloring operator II greatly reduces these spurious currents $(\max \|\vec{u}\|)$, by up to 2 orders of magnitude when the density ratio is high and the surface tension is small. This could explain why there is a large error in the measured surface tension obtained with recoloring operator I.

To obtain convergence with recoloring operator II, the average number of iterations under the stopping criterion with $\epsilon = 10^{-10}$ in Eq. (29) is 73,875. Note that all simulations with recoloring operator I were stopped after 200,000 iterations.

3.3. Layered Poiseuille flow

In the same manner as in Ref. [8], a simulation of a Poiseuille flow between two infinite plates is performed to study the model's ability to simulate two fluids of different viscosity. The simulation is conducted on a lattice containing 1×32 sites (the analytical solution is 1D). The flow is centered at $y = 0$ and is initialized with the red fluid using the zero velocity equilibrium distribution functions for the 16 sites with $y < 0$, and similarly with the blue fluid for $y > 0$. Periodic boundary conditions are used in the x-direction. The first and last sites are used to implement the standard "bounce back" boundary condition. With this condition, the walls are located at $y = -15$ and $y = 15$, which correspond to a channel *half height* of $h = 15$. When implementing the wall boundary condition for the current model, the "density" of the wall must be known

Table 3
Parameters, maximum spurious currents, and errors for the steady bubble test case.

γ	A	ρ_r	R	$\sigma_{predict}$	Recoloring I		Recoloring II	
					$\max \|\vec{u}\|$	E_{I} (%)	$\max \|\vec{u}\|$	E_{II} (%)
1	4e−04	1	20	1.066e−03	1.969e−04	3.36	3.308e−04	1.83
1	4e−04	1	40	1.066e−03	2.242e−04	2.55	2.639e−04	2.65
1	4e−04	6	20	6.400e−03	1.894e−04	3.33	3.308e−04	1.83
1	4e−04	6	40	6.400e−03	2.242e−04	2.54	2.639e−04	2.65
1	1e−02	1	20	2.666e−02	5.360e−03	3.17	1.296e−03	0.58
1	1e−02	1	40	2.666e−02	6.349e−03	2.76	1.299e−03	0.40
1	1e−02	6	20	1.600e−01	5.526e−03	3.30	1.296e−03	0.58
1	1e−02	6	40	1.600e−01	6.349e−03	2.76	1.299e−03	0.40
6	4e−04	1	20	6.222e−04	2.092e−02	84.8	4.493e−04	0.36
6	4e−04	1	40	6.222e−04	1.452e−02	74.3	2.133e−04	1.37
6	4e−04	6	20	3.733e−03	2.017e−02	60.3	4.493e−04	0.36
6	4e−04	6	40	3.733e−03	1.446e−02	88.0	2.133e−04	1.37
6	1e−02	1	20	1.555e−02	2.066e−02	1.51	2.726e−03	2.46
6	1e−02	1	40	1.555e−02	2.543e−02	3.56	2.884e−03	0.80
6	1e−02	6	20	9.333e−02	2.069e−02	1.50	2.726e−03	2.46
6	1e−02	6	40	9.333e−02	2.543e−02	3.47	2.884e−03	0.80

in order to calculate the color gradient. For the current simulation, the top wall is set to be red wet, so $\rho_r = 1$ and $\rho_b = 0$ on the last site. Similarly, the bottom wall is set to be blue wet, with $\rho_r = 0$ and $\rho_b = 1$. The parameters of the simulation are: $\rho_r = 1$, $\gamma = 1$, $A_r = A_b = 0$, $\alpha_b = 0.2$, $v_r = 1/6$, and viscosity ratio $v = \frac{v_r}{v_b}$. For this case, only recoloring operator II converges the solution to steady state, with $\epsilon = 10^{-11}$. The convergence of recoloring operator I is unsatisfactory, because it is similar to the planar interface simulations. For this particular flow, with the "shear viscosities" μ_r and μ_b, and when the compressibility effects are neglected, an analytical solution exists:

$$\begin{aligned} u^r &= \frac{Gh^2}{2\mu_r}\left[-\left(\frac{y}{h}\right)^2 + \frac{y}{h}\left(\frac{\mu_r-\mu_b}{\mu_r+\mu_b}\right) + \frac{2\mu_r}{\mu_r+\mu_b}\right], \quad -h \leqslant y \leqslant 0, \\ u^b &= \frac{Gh^2}{2\mu_b}\left[-\left(\frac{y}{h}\right)^2 + \frac{y}{h}\left(\frac{\mu_r-\mu_b}{\mu_r+\mu_b}\right) + \frac{2\mu_b}{\mu_r+\mu_b}\right], \quad 0 \leqslant y \leqslant h, \end{aligned} \tag{35}$$

where G is the pressure gradient between the two ends of the channel. That pressure gradient is simulated using an equivalent body force, which is implemented by adding G/ω to the horizontal component of the total velocity when computing the equilibrium distribution function $N_i^{k(e)}$ in the operator $(\Omega_i^k)^{(1)}$. Note that the pressure gradient G is chosen to achieve a speed at the center of the channel of $u_c = 0.000045$:

$$G = \frac{u_c(\mu_r + \mu_b)}{h^2} \tag{36}$$

As with the stationary bubble, E_{I} and E_{II} denote the relative error between the theoretical total velocity and the numerical total velocity when a simulation is performed with recoloring operators I and II respectively. For the numerical simulations considered here, it should be noted that the errors obtained are practically the same with both recoloring operators, i.e. $E_{\mathrm{I}} \approx E_{\mathrm{II}}$. Errors at four different positions in the channel are listed in Table 4 for different viscosity ratios.

Fig. 2 shows the numerical solution and the analytical solution when using recoloring operator II and for different viscosity ratios. The solution with recoloring operator I (not shown) is almost the same as the solution with recoloring operator II.

For the chosen parameters, the current model can accurately simulate a high viscosity ratio for the layered Poiseuille flow without any velocity discontinuity at the interface. As in Ref. [36], velocity discontinuity does arise in the current model if the kinematic viscosity of one of the fluids is too high. To solve such a discontinuity in the velocity profile, a two-relaxation-time (TRT) collision operator can be used instead of a simpler BGK operator [37,36].

Based on the results obtained, it can be concluded, for this numerical experiment, that the two recoloring operators behave similarly and lead to a satisfactory solution. The similarity of the results for both recoloring operators is not surprising, since, for the planar interface and steady bubble, the results are also similar when the density ratio is unitary.

3.3.1. Layered Poiseuille flow with density ratios larger than unity

An analytical solution for a layered Poiseuille flow with larger density ratios can be found in the section above, or in Refs. [38,8,36]. In a similar manner as for a unit density ratio, we tried to simulate the flow by adding a body force $\frac{G}{\rho\omega}$ to the equilibrium velocity. The simulation results in a large discrepancy between the numerical and analytical solutions when the density ratio is larger than unity, i.e. a discontinuity arises in the velocity profile at the interface between the fluids. This behavior has also been found in Ref. [36].

The artifice of adding a body force to mimic a pressure gradient may be one cause of the inaccuracy. As pointed out by Buick and Greated [39], adding $\frac{G}{\rho\omega}$ to the equilibrium velocity is less valid in the presence of a density gradient. It is not yet clear to us how to implement a consistent body force with a variable density ratio. Another possible cause of the inaccuracy, mentioned by Rannou [36], may be the inability of the LB model to guarantee a simultaneous continuity of the shear stress and velocity when the density ratio is larger than one. This problem clearly deserves more attention and further research.

In fact, the ability of the current LB model to simulate flow with a density ratio larger than unity is questionable. As shown by Rannou [36], this comment can be made for at least four types of LB model (RK, SC, FE, and MF), for which a discontinuity arises in the velocity profile. We note that this problem has only recently been identified, and, as stated by Aidun and Clausen, it is known as the "discontinuity problem" [40].

Nevertheless, it appears that recoloring operator II corrects the inaccuracy found with recoloring operator I when density ratio is not unity, at least for the planar interface and steady bubble case. In this respect, the multiphase LB community should attempt to successfully simulate layered Poiseuille flow with density ratios larger than unity.

Table 4
Relative errors (%) in the velocity profile at different positions in the channel for the layered Poiseuille flow and different viscosity ratio, v.

v	$y = -7.5$	$y = -0.5$	$y = 0.5$	$y = 7.5$
10	0.0439	0.0343	0.5776	0.3635
100	0.0485	0.0418	2.2146	0.4848
1000	0.0521	0.0464	3.3110	0.5133
10,000	0.0502	0.0442	3.4807	0.5094

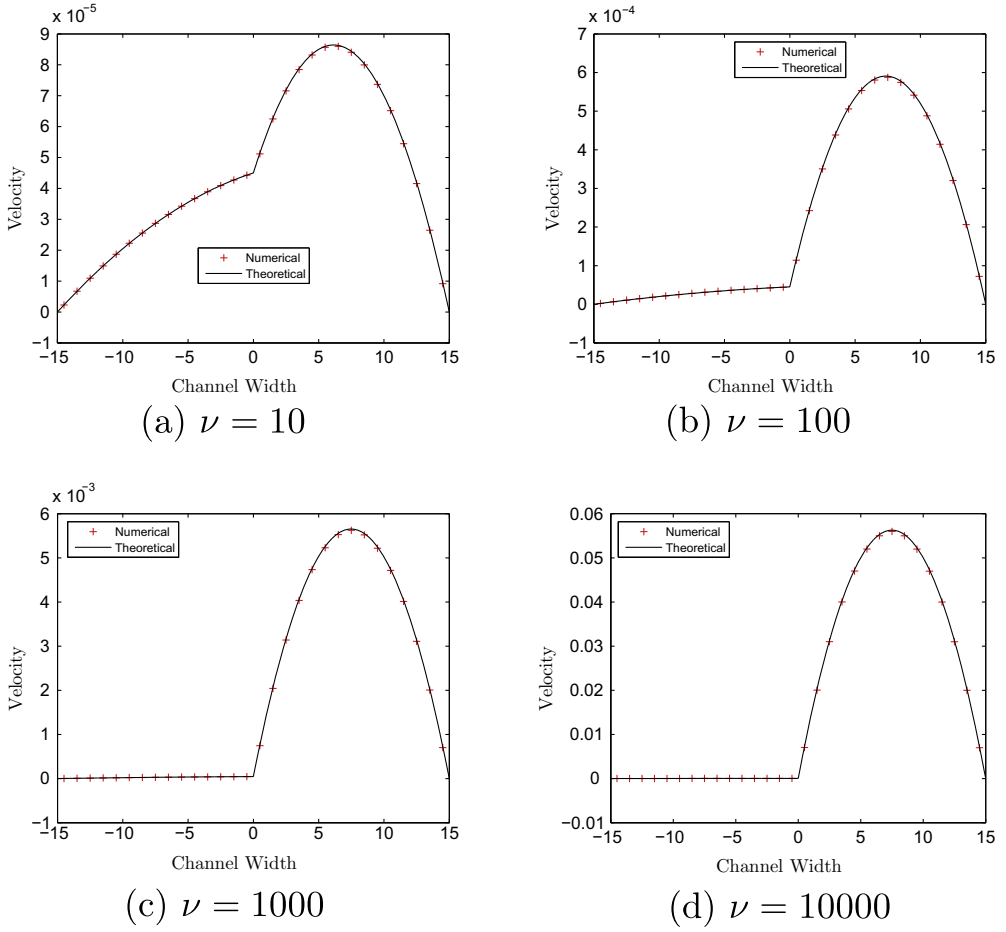

Fig. 2. Numerical and theoretical velocity profile for the layered Poiseuille flow obtained with recoloring operator II and a different viscosity ratio, ν.

3.4. Bubble coalescence

The next numerical experiment involves the coalescence of two bubbles of equal density in a fluid with an equal, lower, or higher density, which is equivalent to a 3D collision of two cylinders of infinite length. This test is used to assess the ability of recoloring operator II to perform an unsteady simulation where a final steady solution exists on which we can measure and predict the final surface tension.

A lattice of 100×100 sites is used, with periodic boundary conditions at the four ends. The computational domain then measures 99 lattice units in both height and width. The corner at the bottom left of the domain is located at the origin (0,0). Using zero velocity equilibrium distribution functions, two red/blue fluid bubbles of radius $R = 18$, with density $\rho_r = 1$ or $\rho_b = \frac{1}{\gamma}$, are initialized at the following respective positions:

$$(x - 49.5)^2 + (y - 49.5 \pm 18)^2 \leqslant 18^2. \tag{37}$$

The remaining sites are similarly initialized with the blue/red fluid, and respecting a certain density ratio γ. The simulation parameters are set with $\alpha_b = 0.6$, $A_r = A_b$, $\sigma_{predict} = 6 \cdot 10^{-3}$, and $\nu_r = \nu_b = 1/6$. "Snapshots" of the color field ψ showing the collision of two dense red bubbles for density ratio $\gamma = 35$ and with recoloring operator II are presented in Fig. 3 for different times. The results shown in Fig. 3 are very similar to those obtained by Reis and Phillips [8]. The reason why they differ qualitatively is that the surface tension in our simulation is about half that in the simulation presented by Reis and Phillips [8].

The fluids are immiscible and a surface tension exists between them. Because of this, at steady state, the surface contact "area" between the two fluids is minimal, and only one big red bubble remains. It is stated in [8] that the final radius of the red fluid bubble should be equal to $R_f = \sqrt{2}R$. Therefore, at steady state, when using this predicted radius, R_f, in the Laplace Eq. (32), the Laplace surface tension obtained, $\sigma_{Laplace}$, should be equal to the predicted surface tension $\sigma_{predict}$ that was set with Eq. (30) at the beginning of the simulation. Simulation of bubble coalescence was performed for different density ratios and with both recoloring operators. Some results are shown in Table 5, with the errors and the pressure calculated as in the steady bubble simulation.

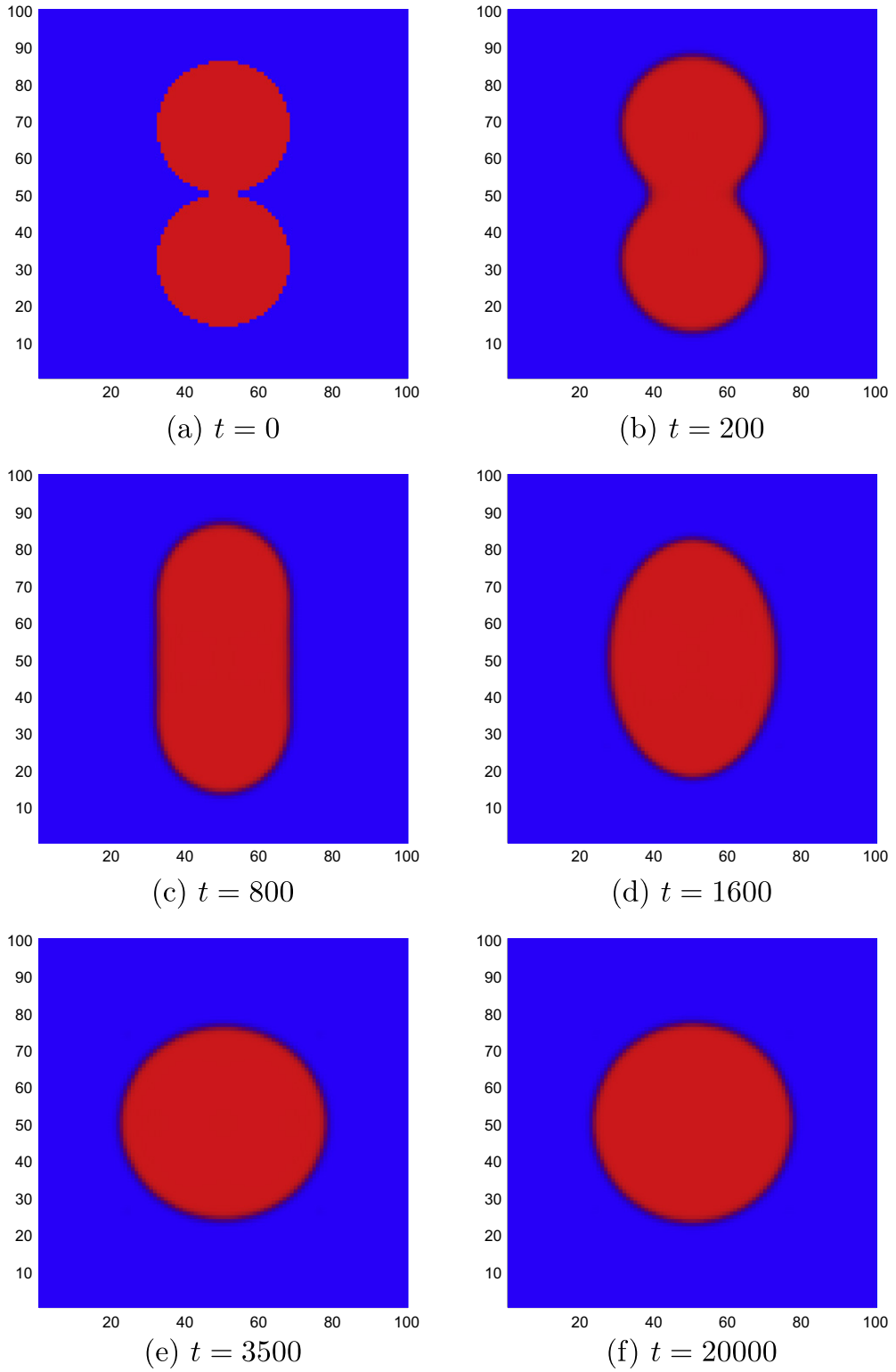

Fig. 3. Collision of two dense red bubbles in a less dense fluid at different times ($\gamma = 35$). (For interpretation of the references to color in this figure legend, the reader is referred to the web version of this article.)

Table 5
Error after the coalescence of the two dense/light bubbles between the predicted and calculated surface tensions $\sigma_{predict}$ and $\sigma_{Laplace}$.

γ	Red dense bubbles		Blue light bubbles	
	E_{I} (%)	E_{II} (%)	E_{I} (%)	E_{II} (%)
1	3.352	0.469	3.352	0.469
35	17.55	3.951	36.06	0.643
40	34.86	4.592	N/A	0.733
45	113.7	5.269	N/A	0.825
50	N/A	5.940	N/A	0.920
80	N/A	11.49	N/A	1.487
85	N/A	12.13	N/A	1.585
90	N/A	N/A	N/A	N/A

The algorithm was stable enough that both recoloring operators were able to simulate a high-density ratio of up to 45. Note that recoloring operator I is unstable for $\gamma = 85$, while recoloring operator II provides a numerically stable solution. As shown in Table 5, recoloring operator II is certainly more accurate and stable than recoloring operator I, as it can achieve error levels smaller than one order of magnitude. Another advantage of recoloring operator II is the economy it generates in terms of computational cost, which is related to the number of time steps needed to arrive at the steady state. The convergence criterion is $\epsilon = 10^{-8}$. To reach the steady-state solution, the mean number of iterations for recoloring operator II is about 46,000, while the simulations carried out with recoloring operator I did not reach convergence at the maximum number of iterations allowed, that is, 200,000.

3.5. Lattice pinning

For the RK model, the pinning problem in multiphase flows has been recognized by several authors: Reis and Dellar [41], Latva-Kokko and Rothman [7], Dupin et al. [42], and Halliday et al. [43,44]. This problem can arise at the interface of two fluids when there is weak convection. In practice, this means that the interface cannot move and becomes "pinned" to the lattice, as long as the convection flow is not strong enough.

To our knowledge, it is unknown whether or not this problem is also present in other type of LB model. In this section, a numerical experiment is proposed to test the presence of lattice pinning. This test, which we could call a tool, may also be applied to other LB schemes to test the presence of pinning.

Although the model of Reis and Phillips is an improvement over others in the same group, the authors indicate that it could suffer from lattice pinning. Latva-Kokko and Rothman have proposed a recoloring algorithm to prevent lattice pinning, or at least diminish it. The next numerical experiment illustrates that combining the two algorithms leads to an improvement in the results.

3.5.1. Numerical experiment 1

The ability of recoloring operator II to reduce the lattice pinning effect is illustrated with the next simulation. A computational domain of 257×33 sites and geometrically located over $[0,-16] \times [256,16]$ is used with periodic boundary conditions in all directions. All sites are initialized with blue fluid using zero velocity equilibrium functions, except that the sites located at $x = 10$ and $y = \pm 8$ are initialized with red fluid. The simulation parameters are $\beta = 0.8$, $\nu_r = \nu_b = 1/6$, $A_r = A_b = 0$, $\rho_r = 1$, and $\gamma = 1$. All simulations are iterated to 10,000 time steps. A body force is added to the fluid, so that it undergoes an acceleration of 0.000005 lattice units per time step squared up to time $t = 6000$. Recoloring operator I is used for all sites, such that $y \geqslant 0$, and operator II is used elsewhere. This configuration allows simultaneous testing of recoloring operators I and II for the lattice pinning problem. The red fluid particle with $y \geqslant 0$ is called red fluid particle I (the same name as the recoloring operator used in this area), and, similarly, the red fluid particle with $y < 0$ is called red fluid particle II. Because there is no surface tension ($A_r = A_b = 0$) and no density or viscosity difference between the two fluids, the horizontal velocity and position of the red fluid particle are the known theoretical ones, given by:

$$\begin{aligned} u_{x,th}(t) &= \begin{cases} \frac{5}{1{,}000{,}000}t, & t < 6000, \\ \frac{3}{100}, & t \geqslant 6000, \end{cases} \\ x_{th}(t) &= \begin{cases} 10 + \frac{25}{10{,}000{,}000}t^2, & t < 6000, \\ 100 + \frac{3}{100}(t - 6000), & t \geqslant 6000. \end{cases} \end{aligned} \tag{38}$$

To compare the numerical results with the analytical results, the average horizontal component of the total fluid velocity of red fluid particles I and II, $u_{x,\mathrm{I}}$ and $u_{x,\mathrm{II}}$, and the average horizontal positions of red fluid particles I and II, x_{I} and x_{II}, are calculated using the color field:

$$
\begin{aligned}
u_{x,\mathrm{I}} &= \langle \{u_x | \psi \geqslant -0.9 \text{ and } y \geqslant 0\} \rangle, \\
u_{x,\mathrm{II}} &= \langle \{u_x | \psi \geqslant -0.9 \text{ and } y < 0\} \rangle, \\
x_{\mathrm{I}} &= \langle \{x | \psi \geqslant -0.9 \text{ and } y \geqslant 0\} \rangle, \\
x_{\mathrm{II}} &= \langle \{x | \psi \geqslant -0.9 \text{ and } y < 0\} \rangle.
\end{aligned} \tag{39}
$$

In Fig. 4 and for $\alpha_b = 0.2$, the average horizontal velocity and position of red fluid particles I and II versus time are presented, together with the analytical solution. In Fig. 4(a), it is apparent that the average horizontal velocities of the two red fluid particles are in agreement with the local fluid flow velocity.

But, Fig. 4(b) clearly shows that recoloring operator I was not able to move the red fluid particle, the position of which did not change over time. When looking at recoloring operator II, the behavior of the particle is much better, because it moves from left to right. Note, however, that lattice pinning has not been avoided completely, because particle II does not move during the first 2000 iterations. In the limit $t \to \infty$, the relative error for the position of the particle diverges to ∞ when recoloring operator I is used, compared to 0% with recoloring operator II. A reduction of parameter β could reduce lattice pinning further, but the interface would become very thick. With this simulation, we can conclude that recoloring operator I reveals a nonexistent physical phenomenon, and that recoloring operator II behaves much better in such a case.

3.5.2. Numerical experiment 2

To further analyze recoloring operator II, the behavior of red fluid particle II is studied as a function of α_b. In theory and without lattice pinning, the integral of the average total fluid velocity of the particle should be equal to the distance traveled, but, when there is lattice pinning, the integrated speed will be greater than the distance traveled. This is because lattice pinning prevents the particle from moving, even if there is a convection current that "tells" it to move.

To approximate the intensity of lattice pinning as a function of α_b, the integral of the total average speed versus time of particle II is compared with the distance traveled. Table 6 indicates the error between the integral of the average speed and the final position of particle II for different values of α_b. The numerical integration is performed with a basic midpoint method using 200 points uniformly distributed between $t = 0$ and $t = 10{,}000$. Although an error is introduced with the numerical integration, it is in the order of the round-off error, because the midpoint method is of second order and the velocity profile is linear in the worst case. The behavior of the error suggests that lattice pinning is reduced with an increasing value of α_b.

For the value of α_b used in Table 6, we can point out that pinning is not prevented at all for recoloring operator I. Because α_b is related to the speed of sound, the results suggest that the slower the speed of sound, the less lattice pinning is taking place.

3.5.3. Numerical experiment 3

Numerical experiment 1 showed that lattice pinning can occur when there is not enough convection and a small red fluid particle is immersed in a blue fluid. This case is extreme, because, initially, the red fluid particle consisted of only a single lattice site, which means that there is a lack of spatial resolution. The next numerical experiment will show that, when the red bubbles cover more lattice sites (better spatial resolution), then the lattice pinning effect disappears and the

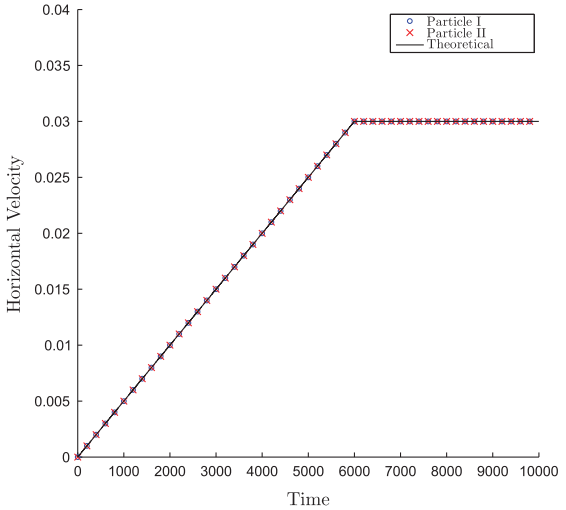

(a) The horizontal velocity as a function of time.

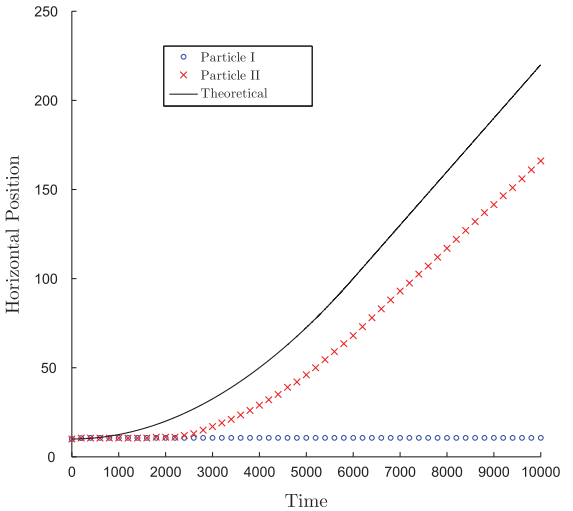

(b) The horizontal position as a function of time.

Fig. 4. Study of the lattice pinning problem.

Table 6
Measure of lattice pinning intensity.

α_b	t = 10,000		$\int_0^{10,000}(u_{x,II})dt$	Error (%)
	$x_{th} - 10$	$x_{II} - 10$		
0.1	210	150.0	210	28.6
0.2	210	156.0	210	25.7
0.4	210	166.5	210	20.7
0.5	210	171.0	210	18.6
0.6	210	175.0	210	16.7
0.8	210	178.0	210	15.2
0.9	210	182.0	210	13.3

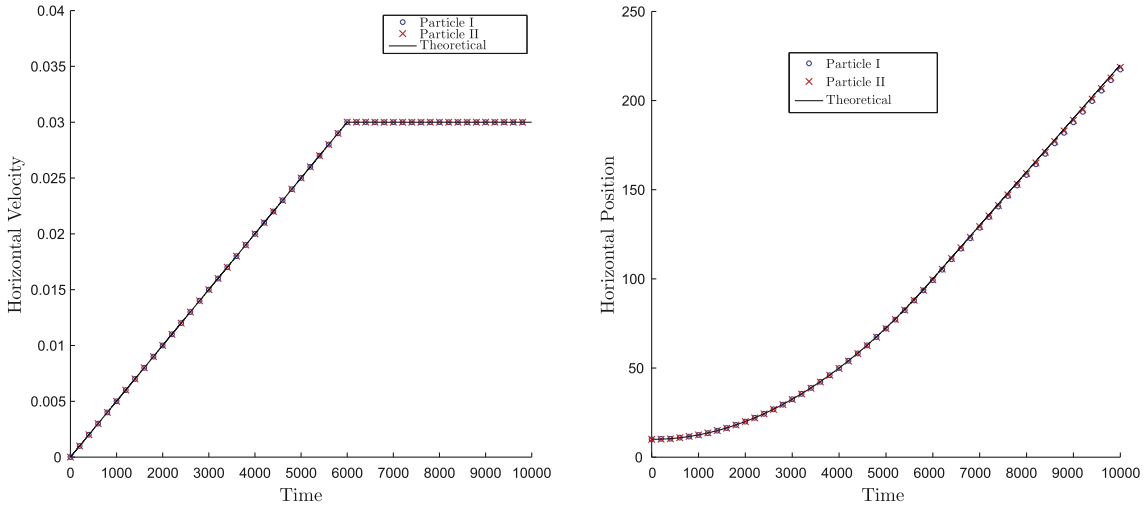

(a) Horizontal velocity as a function of time.

(b) Horizontal position as a function of time.

Fig. 5. Recovery of the analytical solution with a better spatial resolution.

analytical solution is recovered. The setup is as in numerical experiment 1, but with $\beta = 0.99$ and the red fluid zone initially consisting of larger bubbles, with the following equation respected:

$$(x - 10)^2 + (y \pm 8)^2 \leqslant 6^2 \tag{40}$$

Fig. 5 presents the numerical and analytical horizontal velocity and position in such a case. As in numerical experiment 1, and, as expected, in Fig. 5(a), the average horizontal velocities of the two red particles are in agreement with the theoretical solution. For the results obtained in Fig. 5(b), the small error between the numerical solution and the analytical one may come from the way the positions of the red fluid particles are measured, and also, again, from a lack of spatial resolution (even though the results are a great deal better in this numerical experiment). Lattice pinning is a problem that occurs in very particular cases (degenerate), and better spatial resolution appears to fix it for both recoloring operators. It can be concluded that lattice pinning should not be a problem in the majority of the immiscible two-phase flow applications, because, in general, a high enough spatial resolution is chosen to resolve the scale of interest.

However, this is not always possible. For example, in porous media with intricate geometry, a passage could reach the lattice size and the fluid could easily remain (artificially) stuck, impeding the flow. Obviously, this would produce a fake solution. Therefore, it is important to use recoloring operator II instead of operator I for simulating flows for these kinds of media.

4. Conclusion

The Latva-Kokko and Rothman algorithm [7] has been adapted and incorporated into the two-phase lattice Boltzmann model of Reis and Phillips [8]. Numerical simulations were conducted to determine the benefits of such a modification. Simulations of a planar interface, a steady bubble, layered Poiseuille flow, and bubble coalescence showed that the proposed recoloring operator leads to a stationary solution in many fewer iterations than the original recoloring operator use by Reis and Phillips. Regarding accuracy, the two recoloring operators provide similar results for the selected test cases when the density ratio of the two fluids is unity. For the planar interface, and when the density ratio is not unity, the recoloring

operator in [8] introduces a significant error in the surface tension, while the current recoloring operator is very accurate. For the steady bubble simulation, a problem showed up when the density ratio was not unity and the surface tension was low. In that case, the recoloring operator in the Reis and Phillips model introduced a large error in the surface tension, while the present recoloring operator provided satisfactory results. Moreover, the intensity of spurious currents was much lower with the Latva-Kokko recoloring operator than with the recoloring operator in the Reis and Phillips model. For a layered Poiseuille flow problem, the introduction in the model of the recoloring operator of Latva-Kokko and Rothman did not show an improvement over the standard recoloring operator in terms of the accuracy of the results; however, the Latva-Kokko recoloring operator showed an improvement in the number of iterations required to achieve a steady-state solution. A viscosity ratio as high as 10,000 was accurately simulated for the layered Poiseuille flow. We mentioned the discontinuity problem, which is an open problem with the LB model when the density ratio is not unity in the layered Poiseuille flow. This problem definitely needs more attention. In the bubble coalescence simulation, the current recoloring operator showed better numerical stability and accuracy, as the maximum density ratio simulated was 85, which is an improvement over the results in Reis and Phillips's original paper. A simulation conducted to illustrate the problem of lattice pinning revealed that Reis and Phillips's recoloring operator is much more sensitive to this problem than the proposed recoloring operator. For the new model, the numerical results suggest that a low speed of sound can diminish the problem. The last numerical experiment showed that lattice pinning seems to come mainly from a lack of spatial resolution, because, when enough lattice sites are used to define a bubble, the phenomenon disappears. Because, in general, a high enough spatial resolution is chosen to resolve the scale of interest, we can conclude that lattice pinning should not be a problem in the majority of immiscible two-phase flow applications. In conclusion, when the results are compared with those of the Reis and Phillips model [8], the adaptation of the Latva-Kokko and Rothman recoloring operator for this model greatly increases the rate of convergence, improves the numerical stability and accuracy of the solutions over a wide range of model parameters, and significantly reduces the intensity of the spurious currents and lessens the lattice pinning problem.

Acknowledgement

This work was supported by a grant from FQRNT "Le Fonds Québécois de la Recherche sur la Nature et les Technologies".

References

[1] U. D'Ortona, D. Salin, Marek Cieplak, Renata B. Rybka, Jayanth R. Banavar, Two-color nonlinear Boltzmann cellular automata: surface tension and wetting, Phys. Rev. E 51 (4) (1995) 3718–3728.
[2] Daniel H. Rothman, Jeffrey M. Keller, Immiscible cellular-automaton fluids, J. Stat. Phys. 52 (3) (1988) 1119–1127.
[3] Daryl Grunau, Shiyi Chen, Kenneth Eggert, A lattice Boltzmann model for multiphase fluid flows, Phys. Fluids A: Fluid Dyn. 5 (10) (1993) 2557–2562.
[4] A.K. Gunstensen, D.H. Rothman, Microscopic modeling of immiscible fluids in three dimensions by a lattice Boltzmann method, EPL (Europhys. Lett.) 18 (2) (1992) 157–161.
[5] Andrew K. Gunstensen, Daniel H. Rothman, Stéphane Zaleski, Gianluigi Zanetti, Lattice Boltzmann model of immiscible fluids, Phys. Rev. A 43 (1991) 4320.
[6] I. Halliday, S.P. Thompson, C.M. Care, Macroscopic surface tension in a lattice Bhatnagar–Gross–Krook model of two immiscible fluids, Phys. Rev. E 57 (1998) 514.
[7] M. Latva-Kokko, Daniel H. Rothman, Diffusion properties of gradient-based lattice Boltzmann models of immiscible fluids, Phys. Rev. E 71 (2005) 056702.
[8] T. Reis, T.N. Phillips, Lattice Boltzmann model for simulating immiscible two-phase flows, J. Phys. A: Math. Theor. 40 (14) (2007) 4033–4053.
[9] Xiaowen Shan, Hudong Chen, Lattice Boltzmann model for simulating flows with multiple phases and components, Phys. Rev. E 47 (1993) 1815.
[10] Long Wu, Michihisa Tsutahara, Lae Sung Kim, ManYeong Ha, Three-dimensional lattice Boltzmann simulations of droplet formation in a cross-junction microchannel, Int. J. Multiphase Flow 34 (9) (2008) 852–864.
[11] Xiu Qing Xing, David Lee Butler, Sum Huan Ng, Zhenfeng Wang, Steven Danyluk, Chun Yang, Simulation of droplet formation and coalescence using lattice Boltzmann-based single-phase model, J. Colloid Interface Sci. 311 (2) (2007) 609–618.
[12] Xavier Frank, Denis Funfschilling, Noël Midoux, Huai Z. Li, Bubbles in a viscous liquid: lattice Boltzmann simulation and experimental validation, J. Fluid Mech. 546 (2006) 113–122.
[13] T. Inamuro, T. Ogata, F. Ogino, Numerical simulation of bubble flows by the lattice Boltzmann method, Future Gen. Comput. Syst. 20 (6) (2004) 959–964.
[14] Naoki Takada, Masaki Misawa, Akio Tomiyama, Shigeo Hosokawa, Simulation of bubble motion under gravity by lattice Boltzmann method, J. Nucl. Sci. Technol. 38 (5) (2001) 330–341.
[15] Liang Hao, Ping Cheng, Pore-scale simulations on relative permeabilities of porous media by lattice Boltzmann method, Int. J. Heat Mass Transfer 53 (9–10) (2010) 1908–1913.
[16] Jonas Tölke, Lattice Boltzmann simulations of binary fluid flow through porous media, Philos. Trans. R. Soc. Lond. Ser. A: Math. Phys. Eng. Sci. 360 (1792) (2002) 535–545.
[17] A.G. Yiotis, M.E. Kainourgiakis, E.S. Kikkinides, A.K. Stubos, Application of the lattice-Boltzmann method to the modeling of population blob dynamics in 2d porous domains, Comput. Math. Appl. 59 (7) (2010) 2315–2325.
[18] Andreas G. Yiotis, John Psihogios, Michael E. Kainourgiakis, Aggelos Papaioannou, Athanassios K. Stubos, A lattice Boltzmann study of viscous coupling effects in immiscible two-phase flow in porous media, Colloids Surf. A: Physicochem. Eng. Aspects 300 (1–2) (2007) 35–49.
[19] M.M. Dupin, I. Halliday, C.M. Care, Multi-component lattice Boltzmann equation for mesoscale blood flow, J. Phys. A: Math. Gen. 36 (31) (2003) 8517–8534.
[20] Cheng Chen, Dongxiao Zhang, Lattice Boltzmann simulation of the rise and dissolution of two-dimensional immiscible droplets, Phys. Fluids 21 (10) (2009) 103301–103311.
[21] I. Ginzbourg, P.M. Adler, Surface tension models with different viscosities, Transport Porous Med. 20 (1) (1995) 37–76.
[22] Jonas Tölke, Sören Freudiger, Manfred Krafczyk, An adaptive scheme using hierarchical grids for lattice Boltzmann multi-phase flow simulations, Comput. Fluids 35 (8–9) (2006) 820–830.
[23] Hui-dan Yu, Kai-hua Zhao, A new lattice Boltzmann model for two-phase fluid, Chinese Phys. Lett. 16 (4) (1999) 271.
[24] Bo Dong, Y.Y. Yan, Weizhong Li, Yongchen Song, Lattice Boltzmann simulation of viscous fingering phenomenon of immiscible fluids displacement in a channel, Comput. Fluids 39 (5) (2010) 768–779.

[25] Haibo Huang, Zhitao Li, Shuaishuai Liu, Xi-yun Lu, Shan-and-Chen-type multiphase lattice Boltzmann study of viscous coupling effects for two-phase flow in porous media, Int. J. Numer. Methods Fluids 61 (3) (2009) 341–354.
[26] Liang Hao, Ping Cheng, Lattice Boltzmann simulations of liquid droplet dynamic behavior on a hydrophobic surface of a gas flow channel, J. Power Sources 190 (2) (2009) 435–446.
[27] Xiaoyi He, Xiaowen Shan, Gary D. Doolen, Discrete Boltzmann equation model for nonideal gases, Phys. Rev. E 57 (1) (1998) R13.
[28] Xiaoyi He, Shiyi Chen, Raoyang Zhang, A lattice Boltzmann scheme for incompressible multiphase flow and its application in simulation of Rayleigh–Taylor instability, J. Comput. Phys. 152 (2) (1999) 642–663.
[29] L.O.E. Santos, P.C. Facin, P.C. Philippi, Lattice-Boltzmann model based on field mediators for immiscible fluids, Phys. Rev. E 68 (5) (2003) 056302.
[30] Shuling Hou, Xiaowen Shan, Qisu Zou, Gary D. Doolen, Wendy E. Soll, Evaluation of two lattice Boltzmann models for multiphase flows, J. Comput. Phys. 138 (2) (1997) 695–713.
[31] Romana Basit, Abdul M. Basit, Simulation of phase separation process using lattice Boltzmann method, Can. J. Comput. Math. Nat. Sci. Eng. Med. 1 (3) (2010).
[32] C.M. Pooley, K. Furtado, Eliminating spurious velocities in the free-energy lattice Boltzmann method, Phys. Rev. E 77 (4) (2008) 046702.
[33] J. Zhang, D.Y. Kwok, A mean-field free energy lattice Boltzmann model for multicomponent fluids, Eur. Phys. J. – Special Top. 171 (1) (2009) 45–53.
[34] Xiaoyi He, Gary D. Doolen, Thermodynamic foundations of kinetic theory and lattice Boltzmann models for multiphase flows, J. Stat. Phys. 107 (1) (2002) 309–328.
[35] Taehun Lee, Ching-Long Lin, A stable discretization of the lattice Boltzmann equation for simulation of incompressible two-phase flows at high density ratio, J. Comput. Phys. 206 (1) (2005) 16–47.
[36] Guillaume Rannou, Lattice-Boltzmann Method and Immiscible Two-phase Flow, Master's Thesis, 2008.
[37] Irina Ginzburg, Lattice Boltzmann modeling with discontinuous collision components: hydrodynamic and advection–diffusion equations, J. Stat. Phys. 126 (1) (2007) 157–206.
[38] Bhadraiah Vempati, Alparslan Oztekin, Sudhakar Neti, Stability of two-layered fluid flows in an inclined channel, Acta Mech. 209 (3) (2010) 187–199.
[39] J.M. Buick, C.A. Greated, Gravity in a lattice Boltzmann model, Phys. Rev. E 61 (2000) 5307.
[40] C.K. Aidun, J.R. Clausen, Lattice-Boltzmann method for complex flows, Annu. Rev. Fluid Mech. 42 (1) (2010) 439.
[41] T. Reis, P.J. Dellar, A volume-preserving sharpening approach for the propagation of sharp phase boundaries in multiphase lattice Boltzmann simulations, Comput. Fluids 46 (1) (2011) 417–421.
[42] Michael M. Dupin, Ian Halliday, Chris M. Care, Simulation of a microfluidic flow-focusing device, Phys. Rev. E 73 (5) (2006) 055701.
[43] I. Halliday, R. Law, C.M. Care, A. Hollis, Improved simulation of drop dynamics in a shear flow at low reynolds and capillary number, Phys. Rev. E 73 (5) (2006) 056708.
[44] I. Halliday, T.J. Spencer, C.M. Care, Validation of multicomponent lattice Boltzmann equation simulations using theoretical calculations of immiscible drop shape, Phys. Rev. E 79 (1) (2009) 016706.
[45] A.K. Gunstensen, Lattice-Boltzmann studies of multiphase flow through porous media, Dept. of Earth, Atmospheric, and Planetary Sciences, Massachusetts Institute of Technology, (1992), pp. 115–122. Available from: <http://hdl.handle.net/1721.1/13168>.